Supplementary Information for

Variability in storm season intensity modulates ocean acidification conditions in the northern Strait of Georgia

Wiley Evans[1*], Katie Campbell[1], Carrie Weekes[1], Justin Del Bel Belluz[1], Jessy Barrette[1&], Eva Drew Jordison[1], Chris Mackenzie[1], Jonathan Bergshoeff[1], Carolyn Prentice[1], Rosie Savage[1], Isabelle Desmarais[1], Bryn Fedje[1], Emma Myers[1], Kimberly Bedard[1], Alex Hare[1], Ian J. W. Giesbrecht[1], Colleen T. E. Kellogg[1], Zoe Sandwith[1], Jennifer M. Jackson[1#]

[1]Hakai Institute, Heriot Bay, BC, Canada

[*]*Correspondence to: wiley.evans@hakai.org*

[&]*Now at the St. Lawrence Global Observatory, Rimouski, QC, Canada*

[#]*Now at the Institute of Ocean Sciences, Fisheries and Oceans Canada, Sidney, BC, Canada*

Supplementary Text: Estimating freshwater discharge from watersheds draining into the Strait of Georgia

The below tables (Supplementary Tables 1-4) describe the summary statistics of watersheds draining into the Strait of Georgia and information on procedures for estimating discharge in gauged watersheds and ungauged watersheds.

Supplementary Table 1: Inventory of gauges and procedures used to estimate discharge at the outlet of gauged watersheds.

Target	**Gauges summed**	**Gauge for downstream prediction**
Fraser River outlet	08MF005 (Fraser at Hope), 08MG001 (Chehalis), 08MH001 (Chilliwack), 08MH002 (Coquitlam)	08MH001 (Chilliwack)
Squamish River outlet	08GA022 (Squamish near Brackendale), 08GA043 (Cheakamus), 08GA075 (Mamquam)	08GA043 (Cheakamus)
Campbell River outlet	2015-2021: 08HD003 (CR near CR), 08HD005 (Quinsam) 2022 onwards: 08HD035 (CR near cableway)	08HD005 (Quinsam)
Courtenay River outlet	08HB006 (Puntledge), 08HB011 (Tsolum)	08HB011 (Tsolum)
Cowichan River outlet	08HA011 (Cowichan), 08HA003 (Koksilah), 08HA016 (Bings)	08HA016 (Bings)
Oyster River outlet	08HD011 (Oyster), 08HD023 (Little Oyster)	08HD023 (Little Oyster)
Other	NA – only one gauge near the outlet	Same gauge

Supplementary Table 2: Inventory of training gauges used to predict discharge in ungauged watersheds.

Target watershed type	**Training gauges**	**Number of gauges**	**Notes**
GMM	Homathko	1	
SMC	Mean of gauged SMC watersheds*	4	*Campbell omitted because heavily regulated flows are not representative of this watershed type in general. Squamish omitted because it shows a very strong glacial signal not seen in other SMC watersheds
RMC	Mean of gauged SMC watersheds	0	There are no gauges in RMC watersheds of the study area, but watershed characteristics suggest SMC gauges should be reasonably representative.
RHC	Mean of gauged RHC watersheds	9	
RLC	Mean of gauged RLC watersheds	1	

RUC	Mean of gauged RLC watersheds	0	There are no gauged RUC watersheds in the study area, but watershed characteristics suggest RLC gauges should be reasonably representative.

Supplementary Table 3: Gap filling procedures for estimation of rivers discharge. Gaps were filled by adopting the specific discharge of a representative donor gauge in a nearby location.

Gauge with gaps	Donor gauge used to fill gaps	Description of gap	Notes
08HB032 (Millstone)	08GA047 (Roberts Creek)	No data in 2018	Millstone has lowest specific discharge among RHC type but Roberts Ck. often second lowest.
08HB029 (Little Qualicum)	08HB002 (Englishman)	No data in 2018	These are adjacent watersheds with very similar streamflow timing and specific discharge magnitudes.
08HB002 (Englishman)	08HB029 (Little Qualicum)	Missing several months in 2020/2021	These are adjacent watersheds with very similar streamflow timing and specific discharge magnitudes.

Supplementary Table 4: Summary statistics for watersheds of the QU39 drainage area and the subset of Small Coastal Watersheds (SCW). Watershed types and their codes follow Giesbrecht et al.[1,2], except RUC. RUC (Rain UnClassified) watersheds, which were too small to be classified in previous studies, represent low elevation terrain with no glacier cover and a high proportion of precipitation as rain. As such, they are expected to have a rain driven streamflow regime broadly similar to the RLC type. GMM = Glacierized Mountains – Moderately; SMC = Snow Mountains – Central; RMC = Rain Mountains – Central; RHC = Rain Hills – Central; RLC = Rain(shadow) Lowlands – Central.

Watershed type	Count	Total area (km^2)	Mean size (km^2)	% of area	% of SCW area
Fraser	1	232,137	232,136.6	87.7	NA
GMM	17	10,752	632.5	4.1	32.9
SMC	331	13,979	42.2	5.3	42.7
RMC	122	288	2.4	0.1	0.9
RHC	545	5,927	10.9	2.2	18.1
RLC	217	1,389	6.4	0.5	4.2
RUC	1,080	367	0.3	0.1	1.1
Total	*2,313*	*264,839*		*100*	*810*

Supplementary Text: On the relationship between climate indices and cumulative north-south wind stress in the northern Strait of Georgia

It is expected that storm season intensity in the northern Strait of Georgia is governed by large-scale climate conditions. Specifically, storm intensity is likely related to the phase of the North

Pacific Gyre Oscillation (NPGO), Pacific Decadal Oscillation (PDO) or El Niño Southern Oscillation (parameterized here using the Multivariate ENSO Index Version 2 referred to as MEI). This expectation is consistent with analyses that show statistically significant relationships between climate indices and annual chlorophyll anomalies[3], the timing of spring bloom initiation[4] and zooplankton population dynamics[5,6]. However, such relationships with storm season intensity in the Strait of Georgia have received less attention. To date there has been a single analysis between wind conditions in the central Strait of Georgia (using Environment and Climate Change Canada Halibut Bank weather buoy data) during the storm season (averaged from January to May) and annual mean climate indices[4]. This analysis revealed a statistically significant relationship between NPGO and PDO ($p < 0.01$) and the average wind speed cubed (representing the average energy input to the surface ocean from the winds, or the average wind power) using data from 2003 to 2016. We conduct a similar analysis below using data from the northern Strait of Georgia (from the Environment and Climate Change Canada Sentry Shoal weather buoy) from 1997 to 2024 (Supplementary Figure 1).

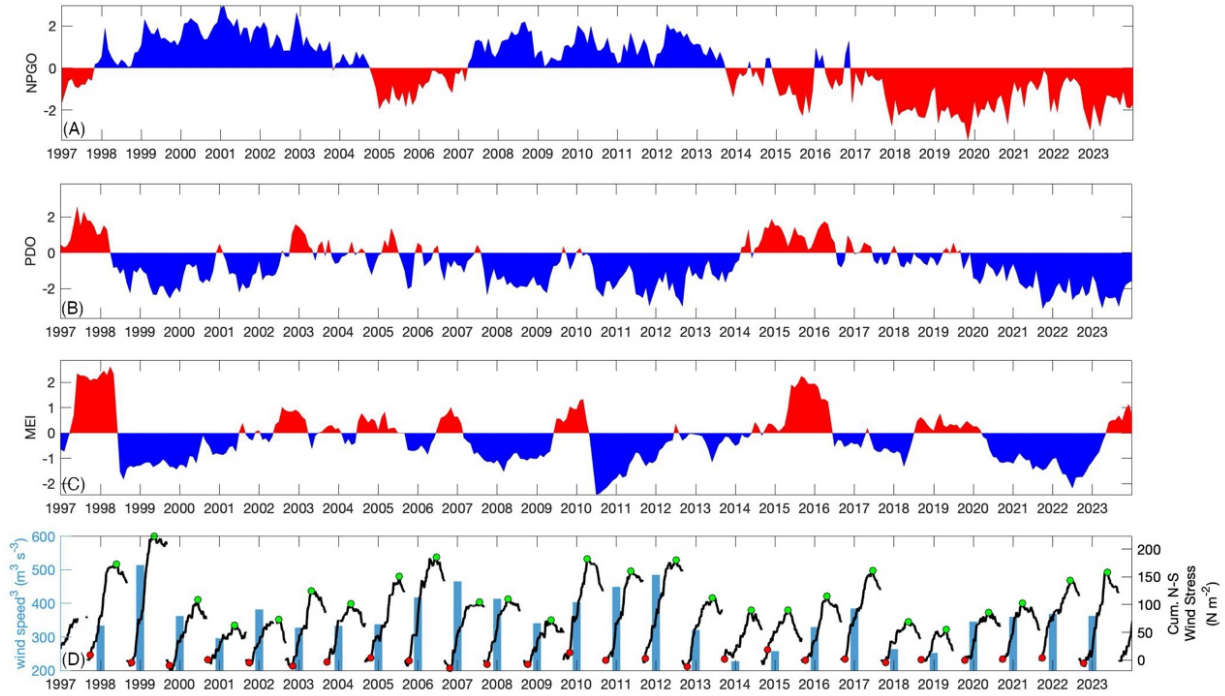

Supplementary Figure 1: Climate indices and winds in the northern Strait of Georgia from 1997 to 2024. (A) The North Pacific Gyre Oscillation (NPGO). (B) The Pacific Decadal Oscillation. (C) The Multivariate ENSO Index Version 2 (MEI). For (A), (B) and (C), warm phase conditions (-NPGO, +PDO, and +MEI) are colored red. Data for (A), (B) and (C) were obtained from https://www.o3d.org/npgo/, https://www.ncei.noaa.gov/access/monitoring/pdo/, and https://psl.noaa.gov/enso/mei/, respectively. (D) The average wind speed cubed during the storm season (blue bars) and the cumulative north-south wind stress (N m^{-2}) from the Environment and Climate Change Canada Sentry Shoal weather buoy. Sources for the Sentry Shoal weather buoy data are provided in the main text.

We first considered the relationship between the cumulative wind stress (CWS) and the average wind speed cubed during the storm season (Supplementary Figure 2). There was a significant relationship between these variables although with appreciable scatter that resulted in an r^2 of 0.56. While particular years, such as 1999, had equally high storm season CWS and average wind speed cubed, there are notable deviations during other years (Supplementary Figure 1). Generally, when there is an intense storm season with high CWS, there is a high average wind power.

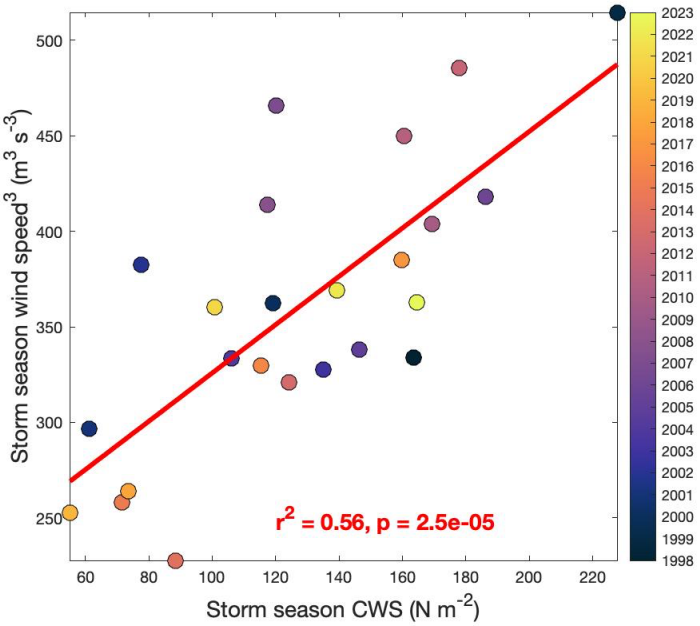

Supplementary Figure 2: The relationship between storm season cumulative wind stress (CWS; N m^{-2}) and the average wind speed cubed over the storm season (m^3 s^{-3}).

There was a notable difference in the statistical significance of the relationships between the climate indices and the CWS and storm season wind speed cubed (Supplementary Table 5). While the directionality of the relationships between storm season variables and climate indices was consistent, the average wind speed cubed over the storm season exhibited significant statistics with each annual mean climate index. The relationships between CWS and the climate indices were not statistically significant, although the computation time frame impacted the statistics and this suggests a longer record length may lead to significant statistics (Supplementary Table 5). These data do suggest that there is a tendency toward more intense storm seasons during cool PDO and ENSO phases.

Supplementary Table 5: Statistics (r and p values) for the regressions between annual mean climate indices (NPGO, PDO, and MEI) and storm season cumulative wind stress (CWS) and average wind speed cubed from 1998 to 2023. Significant regressions at the $p < 0.05$ level are in bold text. Also included are the relationships with PDO for the time frame used in a central Strait of Georgia analysis (2003-2016)[4].

	NPGO (Jan-Dec)	PDO (Jan-Dec)	PDO (Jan-Dec; 2003-2016)	MEI (Jan-Dec)
Storm season CWS	r = 0.25, p = 0.25	r = -0.37, p = 0.06	r = -0.48, p = 0.08	r = -0.36, p = 0.07
Storm season wind speed^3	**r = 0.42, p = 0.03**	**r = -0.58, p = 1.9x10^{-3}**	**r = -0.76, p = 1.6x10^{-3}**	**r = -0.56, p = 3.3x10^{-3}**

Supplementary Text: Conservative relationships for alkalinity and TCO_2

The regional alkalinity-salinity relationship presented in Evans et al[7] was updated to include more recent data from oceanographic station QU39. The relationships between TCO_2 and salinity were also developed using these data. These relationships were used to evaluate the role of conservative mixing in the seasonal and inter-annual decompositions of $\Delta\Omega_{cal}$.

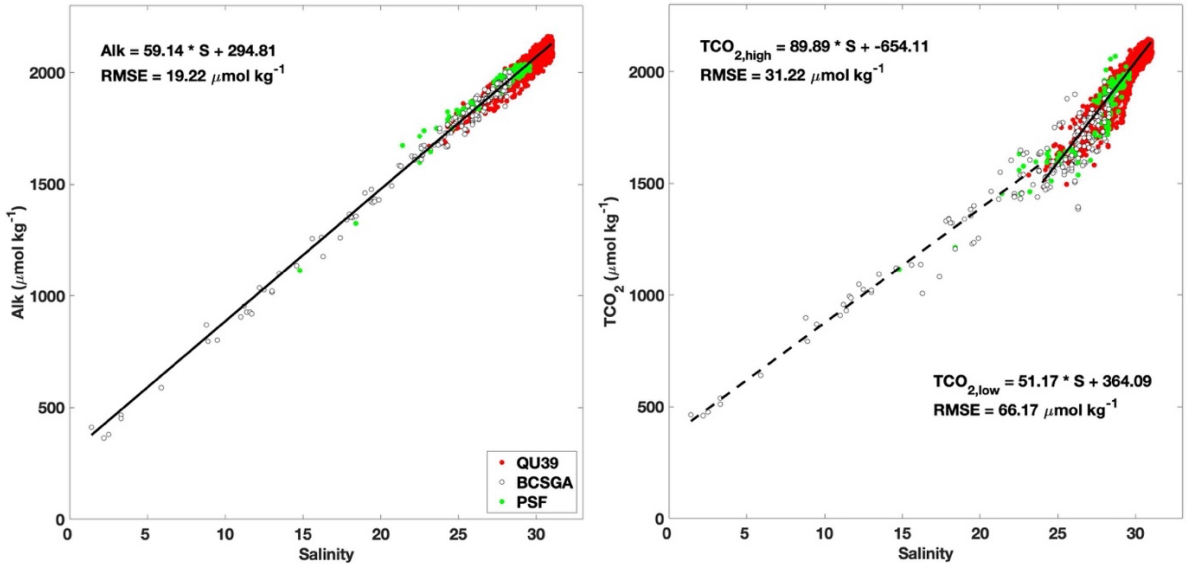

Supplementary Figure 3: Conservative relationships for alkalinity (left; µmol kg^{-1}) and TCO_2 (right; µmol kg^{-1}). Data included here are from QU39 (red) and measurements broadly collected in the region by the Pacific Salmon Foundation (green; https://catalogue.hakai.org/dataset/ca-cioos_3d7d93d0-73be-4c1b-af09-307e60a3576d) and the British Columbia Shellfish Growers Association (white; https://catalogue.hakai.org/dataset/ca-cioos_a72c43e2-5b4d-4d56-89d4-464b4c513710). The cut-off for the high and low TCO_2 relationships was at a salinity of 24.

Supplementary Text: TCO_2 and pCO_2 measurement quality control and uncertainty assessment

The following describes the quality control (QC) procedure for measurements of total dissolved inorganic carbon (TCO_2) and carbon dioxide partial pressure (pCO_2) made on discrete seawater samples collected using Niskin bottles and analyzed using a Burke-o-Lator TCO_2/pCO_2 Analyzer[8]. The approach to evaluate measured and derived marine CO_2 system parameter uncertainties is also described. The below steps extend from the evaluation of Excel worksheet calculations completed during sample analysis[8] and routines described in provided code on GitHub (https://github.com/HakaiInstitute/Discrete-CO2-Processing-Code?tab=readme-ov-file). Note that TCO_2 measurements would have been evaluated and deemed "good" or "questionable" during the evaluation of Excel worksheets by examining correction factors (acceptable values within 1±0.01) and the standard deviation of triplicate reference material analyses.

Concatenation and initial quality checks using CTD data

The first step in examining the quality of TCO_2 and pCO_2 measurements from an oceanographic field campaign was to produce a "master file" of concatenated data from the Excel worksheets generated during sample analysis and the corresponding sample logs completed during sample collection. Information generated during sample collection included

collection date and time, latitude, longitude, depth, sample temperature at the time of collection, and any notes related to Niskin bottle integrity checks and sample collection. Each sample in the master file was initially given a data quality flag of "1" if considered a good measurement, or "2" if part of a replicate series (usually a triplicate set), or "4" if not analyzed. Further evaluation of data quality, and the adjustment of flags "1" or "2" to flag "3", representing a questionable measurement, occurred in the following steps.

The next data-handling step involved merging conductivity-temperature-depth (CTD) profile data with the master file and then doing comparisons between select measurements. Note that available nutrient data were also merged with the master file, although these data were not used in CO_2 system calculations. Data merging consisted of matching date, latitude, longitude, and depth between the discrete TCO_2/pCO_2 samples collected with Niskin bottles and 1-m bin-averaged CTD data. Note that CTD profiling and Niskin bottle sampling occurred sequentially during our small boat surveys. After CTD data were merged with the master file, the sample temperature at the time of collection (recorded using a NIST-traceable probe) and the sample salinity (measured in the laboratory with a YSI conductivity cell that was calibrated using certified reference materials from Andrew Dickson at UCSD) were compared with the CTD temperature and salinity recorded at the depth the Niskin bottle was tripped (determined using an RBR Solo pressure sensor attached to each Niskin bottle, or line out markers if no pressure measurement was available). All salinity units were reported on the Practical Salinity Scale - 1978. The comparison between NIST temperature and CTD temperature was useful for evaluating the degree of warming that may have occurred between recovering the Niskin bottle and drawing the sample; however, this warming was typically minimal. The comparison between sample and CTD salinity was examined for large differences that would indicate a sample collection issue, such as a sample drawn from the wrong Niskin bottle or a Niskin bottle tripped at the wrong depth. Samples that exceeded 8 times the root mean square error (RMSE) of the linear relationship between sample and CTD salinity (a typical RMSE value is 0.12) received a flag of "3". This large exceedance threshold was used to account for the expected high variance between CTD and discrete sample salinity within the surface layer.

Quality control of pCO_2 measurements

Following the comparison to CTD data, we utilized a regional alkalinity-salinity relationship[7] to help identify questionable measurements of pCO_2 recorded at the analysis temperature (pCO_2@analysisT). Implicit here was the assumption that analytical errors in the TCO_2 measurement will have been identified during the evaluation of Excel worksheet calculations[8]. Therefore, flag "1" TCO_2 measurements could be combined with salinity-determined alkalinity to derive pCO_2, and this derived pCO_2 could then be compared with pCO_2@analysisT to isolate questionable measurements. A second assumption here is that the regional alkalinity-salinity relationship was robustly constrained with minimal non-conservative character in alkalinity[7]. If a pCO_2 measurement appeared questionable, a large difference manifested between pCO_2@analysisT and the derived value; however, the extent of this difference was dependent on the buffering state of the sample (*i.e.*, the ratio between alkalinity and TCO_2).

To aid in evaluating the difference between measured and derived pCO_2 across a wide range of buffering states, we utilized the uncertainty of the regional-alkalinity salinity relationship (characterized by the root mean square error; RMSE) to create a hypothetical pCO_2 threshold. We considered two cases: (1) seawater containing high TCO_2 (nominally 2100 µmol

kg^{-1} for oceanographic station QU39), and (2) seawater containing low TCO_2 (nominally 1600 $\mu mol\ kg^{-1}$). Constant temperature and salinity values of 18.7°C and 29.6 (median analysis temperature and sample salinity in the QU39 dataset), respectively, were used to create the hypothetical pCO_2 thresholds for each case. Alkalinity was calculated for a range of alkalinity and TCO_2 ratios (Alk:TCO_2 from 0.9 to 1.4) for both cases. Then the RMSE of the regional alkalinity-salinity relationship (22.47 $\mu mol\ kg^{-1}$) was either added to or subtracted from alkalinity to derive high or low pCO_2 values across the range of Alk:TCO_2 ratios for the high and low TCO_2 cases. The difference between high and low pCO_2 values reflects uncertainty in derived pCO_2 across the range of Alk:TCO_2 ratios, and was similar between the high and low TCO_2 cases. The difference between high and low pCO_2 values across the range of Alk:TCO_2 ratios was then scaled up by a factor of 2 in order to account for divergences from the regional alkalinity-salinity relationship and the constant temperature and salinity values, and then these scaled values were used as the hypothetical pCO_2 threshold to isolate questionable measurements (Supplementary Figure 4).

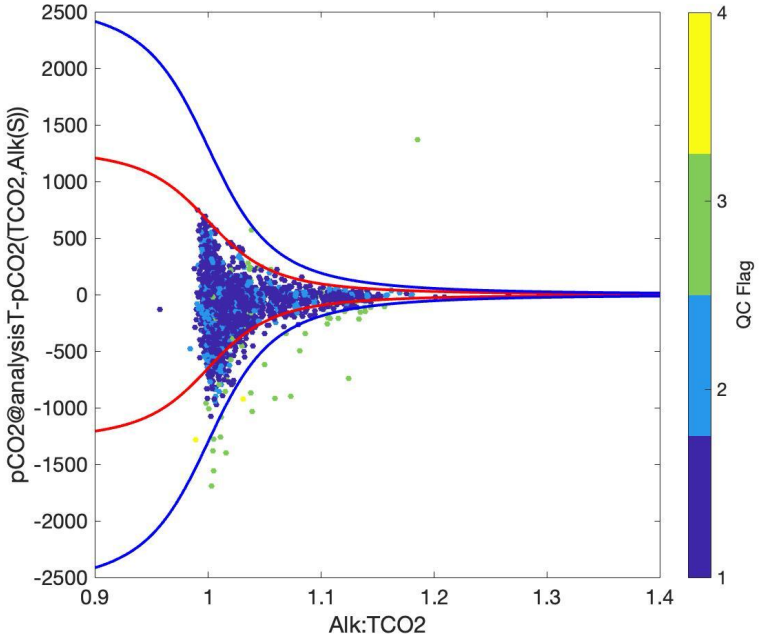

Supplementary Figure 4: The flagging of pCO_2@analysisT that exceeded a hypothetical pCO_2 threshold across a range of Alk:TCO_2 ratios (blue lines). The red lines are the theoretical differences between pCO_2(TCO_2, Alk(S)+RMSE) and pCO_2(TCO_2, Alk(S)-RMSE) and the blue lines are those differences scaled up by 2. Data points are pCO_2@analysisT minus pCO_2(TCO2,Alk(S)), and values outside of the range of the blue lines were identified as questionable and given a flag of "3".

Final quality control evaluation

Final checks of the data quality involved plotting the derived alkalinity versus salinity and examining assorted property plots. In a region where the relationship between alkalinity and salinity is linear across the range of observations (as opposed to sites or surveys that encompass deep samples from off the continental shelf that may have two linear regions in an alkalinity-salinity plot; *i.e.*, a "hockey stick" curve) and robust, this check can be used to identify outliers that may represent questionable data not captured by the above steps. Property versus time plots

(for pCO_2 and alkalinity) for each sampling depth (*i.e.*, treating each sampling depth as a distinct time series), property versus depth plots (for pCO_2, TCO_2, and alkalinity), and property versus property plots (TCO_2 versus oxygen, pCO_2 versus oxygen, and TCO_2 versus nitrite plus nitrate) were used to evaluate the dataset for missed outliers. Finally, triplicate measurements were statistically evaluated (below) with medians retained for the final dataset, and quality control flag values were adjusted to conform to conform to a WOCE-style flagging scheme[9] (2 = acceptable, 3 = questionable, 6 = median of replicates, 9 = missing value).

Evaluating TCO_2 and pCO_2 measurement uncertainty

As mentioned above, TCO_2 measurements were corrected using results from reference material analyses done in triplicate at the start and end of a series of seawater sample analyses consisting of approximately 20 samples[8]. Correction factors were applied to each seawater measurement by first dividing the reported TCO_2 content of the reference material by the average from each triplicate analysis of certified reference material that bracketed the seawater sample analyses and then interpolating those values to the seawater measurement time points. Reference materials used were either certified reference material (CRM) from Andrew Dickson (UCSD) or internal reference material (IRM) consisting of mixtures of sodium carbonate and sodium bicarbonate in deionized water that had been analyzed alongside CRMs to determine their TCO_2 content. The standard deviation of each triplicate analysis series of reference materials provided a metric for the analytical uncertainty of the TCO_2 measurement. The median standard deviation of 582 triplicate analyses of CRMs was 6.2 μmol/kg with a median-centered coefficient of variation (CV) of 0.3%. This is identical to the relative uncertainty for TCO_2 measurements reported by Evans et al[7]. The median standard deviation of 294 triplicate analyses of IRMs was 3.3 μmol/kg with a median-centered CV of 0.2%. Combining the median-centered CVs from CRM and IRM analyses in quadrature results in a value of 0.36%, which we take to be the relative uncertainty for our TCO_2 analyses (*i.e.*, the analytical uncertainty).

We currently lack reference materials for seawater pCO_2 analysis. The uncertainty of pCO_2 analyses was previously evaluated by analyzing CRMs for both TCO_2 and pCO_2, then deriving alkalinity, and finally comparing those derived values to the certified CRM values[7]. The difference between derived and certified alkalinity was typically within 1.5% and taken to be the relative uncertainty in the measurement. However, this value includes uncertainties in both of the TCO_2 and pCO_2 measurements and the CO_2 equilibrium constants. Additionally, the TCO_2 analytical uncertainty reported above does not include uncertainty that can occur during sample collection. We therefore incorporate results from 198 triplicate sets of seawater samples collected randomly across sampling depths at oceanographic station QU39 to provide an additional assessment of TCO_2 measurement uncertainty and a more robust estimate of pCO_2 measurement uncertainty. Supplementary Figure 5 shows CV values from the 198 triplicate sets of seawater samples with the median value for each record taken as a measure of the combined uncertainty from sampling and analysis. This value for pCO_2 was 1.2%, slightly lower than from the value reported previously[7]. The value for TCO_2 was 0.21% and was slightly lower than the assessment from reference material triplicates above. In order to produce a more conservative estimate of TCO_2 measurement uncertainty, we combined this value with the median CV from the triplicate reference material assessment in quadrature to produce a measure of total (*i.e.*, analytical plus sampling) relative uncertainty; this value was estimated to be 0.42% for our discrete seawater TCO_2 measurements and deemed to be "weather quality"[10].

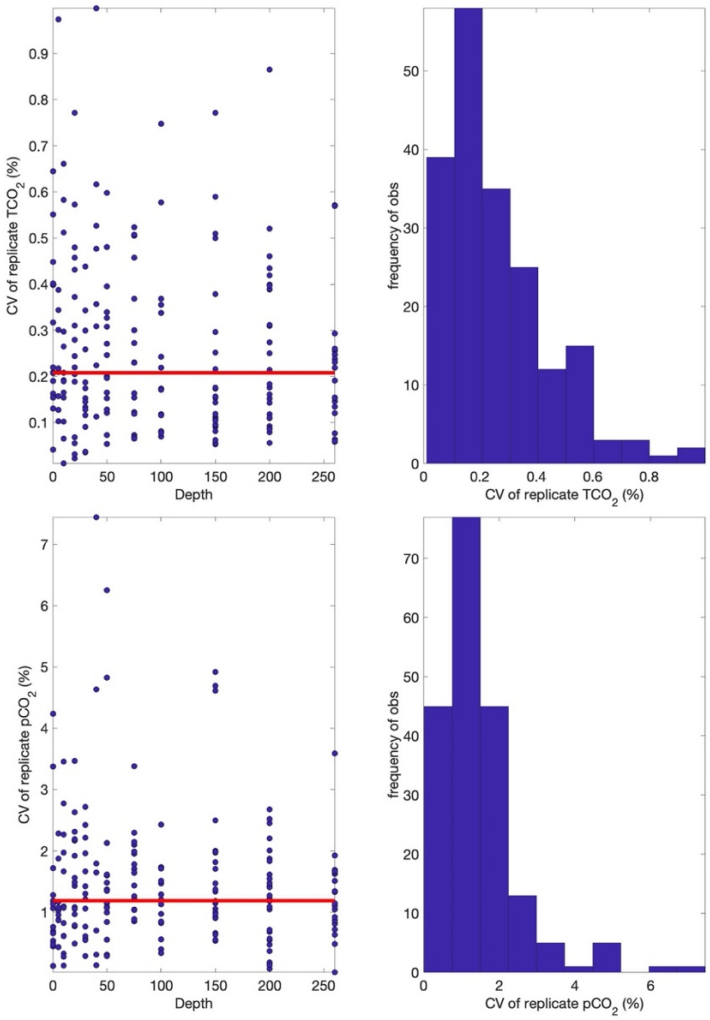

Supplementary Figure 5: Median-centered coefficient of variation (CV) values from 198 triplicate sets of seawater TCO_2 (top) and pCO_2 (bottom) measurements. Left panel shows CV values versus sampling depth with the red horizontal line representing the median CV value in the record. The right panel shows the frequency distribution of CV values. The median CV value for each record is taken as a measure of uncertainty (0.21% for TCO_2; 1.2% for pCO_2).

Derived marine CO_2 parameter uncertainty

The conversion to *in situ* pCO_2 conditions (*i.e.*, at the temperature and pressure the sample was collected) and the calculation of the remaining marine CO_2 system parameters, *e.g.*, alkalinity, pH reported here on the total scale (pH_T), and aragonite and calcite saturation states, required a two-step process owing to the fact that the pCO_2 measurement utilized equilibration with a headspace gas and this process slightly alters the TCO_2 content of the sample. A headspace gas correction was applied to the TCO_2 measurements[11], which incorporated measurements of the headspace gas prior to equilibration (*i.e.*, an atmospheric pCO_2 measurement, nominally near 400 µatm), the seawater volume of the sample (325 ml), and the headspace gas volume (90 ml). Headspace gas-adjusted TCO_2 data were then used with the pCO_2 measurements to derive the seawater alkalinity using the carbonic acid dissociation constants from Waters et al[12], the bisulfate dissociation constant from Dickson et al[13], the fluoride and hydrogen association constants from Perez and Fraga[14], and the boron / chlorinity ratio from

Uppström[15]. Alkalinity was considered here to consist of carbonate, bicarbonate, borate, hydroxide and hydrogen ions as determined using CO2SYS software (Matlab v3.0)[16]. Uncertainty in all derived parameters was evaluated using the error.m routine from Orr et al[17]. To estimate the uncertainty of derived alkalinity, uncertainties were propagated from the pCO_2 measurement and the headspace gas-adjusted TCO_2. Uncertainty in headspace gas-adjusted TCO_2 was taken to be equivalent to the TCO_2 measurement uncertainty despite the headspace gas adjustment having uncertainty associated with primarily the atmospheric measurement (~2 µatm) and the headspace gas volume (~2%). Typical adjustments are on the order of 1 µmol/kg and the uncertainty amounted to roughly 2% of the adjustment, and therefor was considered negligible. Supplementary Figure 6 shows the resulting uncertainty in derived alkalinity as a function of TCO_2. We take the median value to represent our typical uncertainty for derived alkalinity, albeit note larger spread in the uncertainty in derived alkalinity at lower TCO_2 content.

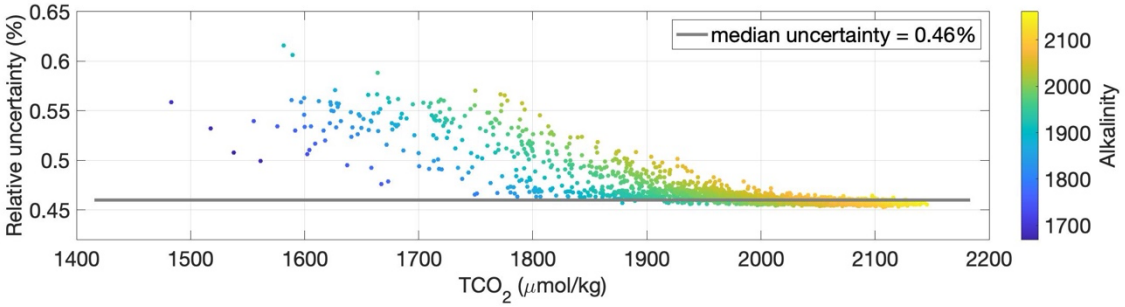

Supplementary Figure 6: Relative uncertainty in seawater alkalinity (%) as a function of TCO_2 content (µmol/kg) with color as the derived alkalinity content. The typical uncertainty of derived alkalinity was 0.46% and was represented by the median value.

After deriving alkalinity, the pCO_2, pH_T, and carbonate mineral saturation states were calculated at *in situ* temperature, salinity, and pressure using the same suite of marine CO_2 system constants. This calculation was done using CO2SYS with derived alkalinity and measured TCO_2. However, it is important to note that evaluating the uncertainty of these terms using the derived alkalinity and measured TCO_2 uncertainties would result in double-counting the measured TCO_2 uncertainty. Therefore, we evaluate the uncertainty in pCO_2, pH_T, and carbonate mineral saturation states at in situ conditions using the uncertainties in our direct measurements, pCO_2 and TCO_2, in addition to uncertainty in the dissociation constants. Uncertainty in these derived parameters was evaluated as before by propagating the uncertainties of the input parameters. The median uncertainty values for pCO_2, pH, and calcite saturation state were 1.5%, 0.012, and 4.8%, respectively. Note that we report the absolute uncertainty for pH_T because it is a logarithmic variable; an absolute uncertainty in pH represents a relative uncertainty in hydrogen ion content[17]. We take the median values to reflect our typical uncertainties for these variables. To provide additional context for these estimates of uncertainty, we prescribed the "weather quality" threshold of 10 µmol/kg for TCO_2 and alkalinity[10] to the data used to create Supplementary Figure 7. This assessment highlights that our data quality is within the "weather quality" threshold, as well as our assessment of calcite saturation state uncertainty is close to the 4% uncertainty in aragonite saturation states reported in another study using the same instrumentation[18].

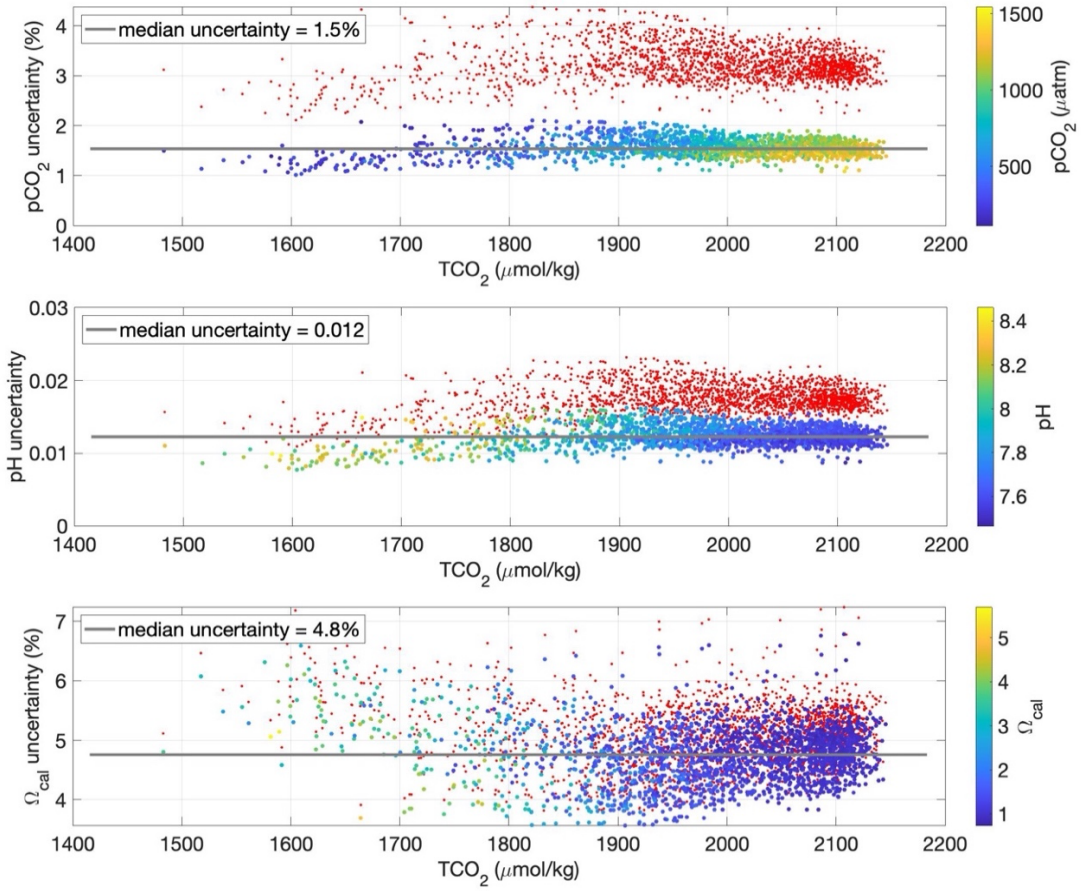

Supplementary Figure 7: Uncertainty in pCO_2 (top; relative %), calcite saturation states (Ω_{cal}; middle; relative %), and pH_T (bottom) as a function of TCO_2 content (µmol/kg) with color indicating the corresponding derived parameter values. Also shown as red dots are parameter uncertainties calculated with prescribed GOA-ON "weather" thresholds for pCO_2 and TCO_2, respectively. As indicated using median values, typical pCO_2, Ω_{cal}, and pH_T uncertainty was 1.5%, 4.8% and 0.012, respectively.

Examining deviations in the global calcium-salinity relationship

We wanted to consider the potential for local deviations in the global calcium-salinity relationship used within the CO2SYS software as an additional source of uncertainty for saturation state determinations[19]. Calcium samples were collected during two surveys at oceanographic station QU39 and used to examine this potential. We lack local freshwater data to build a robust regional relationship, but we do note from this comparison that there is a slight tendency to over-estimate saturation state without better regional constraint of the calcium content. The degree of this over-estimate is approximately 0.04 based on these limited data.

Supplementary Table 6: The difference between measured and calculated calcium content using CO2SYS and the impact on derived aragonite saturation states. The measurements were made on December 1, 2020 (Date 1) and December 17, 2020 (Date 2). The average difference between derived aragonite saturation states using measured calcium or calcium calculated in

CO2SYS was -0.04, suggesting a slight offset in saturation states derived using the global calcium-salinity relationship within CO2SYS.

		[Ca^{2+}], mol kg^{-1}			Calculated ΩAr		
Date	Depth	YSI_S	Measured	CO2SYS	Meas.[Ca^{2+}]	CO2SYS	Diff
1	0	28.1	0.00830	0.00827	0.919	0.914	0.005
1	0	28.1	0.00806	0.00827	0.892	0.914	-0.022
1	5	28.2	0.00806	0.00830	0.854	0.879	-0.024
1	10	28.5	0.00830	0.00839	0.889	0.897	-0.008
1	20	28.6	0.00805	0.00842	0.842	0.878	-0.037
1	30	28.7	0.00805	0.00845	0.833	0.872	-0.039
1	40	28.8	0.00805	0.00848	0.808	0.849	-0.041
1	50	29.1	0.00805	0.00856	0.671	0.713	-0.042
1	75	30.2	0.00853	0.00889	0.579	0.602	-0.023
1	100	30.7	0.00877	0.00903	0.598	0.615	-0.017
1	150	30.9	0.00877	0.00909	0.607	0.629	-0.022
1	200	31	0.00876	0.00912	0.635	0.660	-0.025
1	260	31.1	0.00900	0.00915	0.645	0.655	-0.010
2	0	27.5	0.00782	0.00809	0.821	0.849	-0.028
2	0	27.5	0.00757	0.00809	0.795	0.849	-0.053
2	5	27.7	0.00782	0.00815	0.803	0.836	-0.033
2	10	28.1	0.00781	0.00827	0.776	0.821	-0.044
2	20	28.3	0.00757	0.00833	0.756	0.831	-0.075
2	30	28.4	0.00757	0.00836	0.747	0.824	-0.077
2	40	28.5	0.00757	0.00839	0.751	0.831	-0.080
2	50	28.8	0.00756	0.00848	0.645	0.722	-0.077
2	75	30.3	0.00804	0.00892	0.566	0.627	-0.061
2	100	30.6	0.00828	0.00901	0.567	0.615	-0.048
2	150	30.9	0.00828	0.00909	0.582	0.638	-0.056
2	200	31	0.008	0.578	0.009	0.636	-0.058
2	260	31.1	0.008	0.582	0.009	0.643	-0.061

Supplementary Text: Definition of composite annual cycles

Composite annual cycles were produced for select parameters measured by the conductivity, temperature, depth profiler and for the marine CO_2 system measurements. Gap-filling was necessary to produce composite annual cycles that spanned the entire year because oceanographic surveys began each year after the start of January and ended each year around the middle of December. Supplementary Figure 8 provides an example for how these gaps at the start and end of the year where filled.

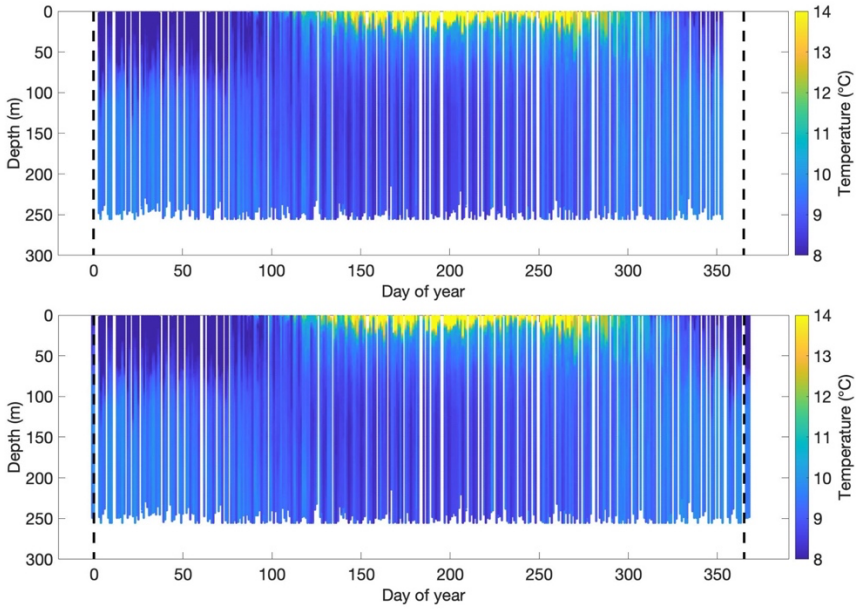

Supplementary Figure 8: The top and bottom panels showcase an example of the gap-filling approach used to produce composite annual cycles. Both panels show profiles of seawater temperature to a depth of 255 m at QU39 in the northern Strait of Georgia. The top panel shows all the profiles within the QU39 data record plotted as a function of day of year with gaps at the start and end of the year. The bottom panel shows these gaps filled by: (1) duplicating the first 15 days of data and moving these duplicated data to the end of the record, and (2) duplicating the last two days of data and moving these duplicated data to the start of the record.

References

1 Giesbrecht, I. J. W. *et al.* Watershed Classification Predicts Streamflow Regime and Organic Carbon Dynamics in the Northeast Pacific Coastal Temperate Rainforest. *Global Biogeochemical Cycles* **36**, https://doi.org/10.1029/2021GB007047 (2022).

2 Giesbrecht, I. *et al.* (DRYAD, in prep).

3 Suchy, K. D., Le Baron, N., Hilborn, A., Perry, R. I. & Costa, M. Influence of environmental drivers on spatio-temporal dynamics of satellite-derived chlorophyll *a* in the Strait of Georgia. *Progress in Oceanography* **176**, 10.1016/j.pocean.2019.102134 (2019).

4 Suchy, K. D., Young, K., Galbraith, M., Perry, R. I. & Costa, M. Match/Mismatch Between Phytoplankton and Crustacean Zooplankton Phenology in the Strait of Georgia, Canada. *Frontiers in Marine Science* **9**, doi: 10.3389/fmars.2022.832684 (2022).

5 Mackas, D. *et al.* Zooplankton time series from the Strait of Georgia: Results from year-round sampling at deep water locations, 1990-2010. *Progress in Oceanography* **115**, 129-159 (2013).

6 Perry, R. I. *et al.* Zooplankton variability in the Strait of Georgia, Canada, and relationships with the marine survival of Chinook and Coho salmon. *PLoS ONE* **16**, e0245941, doi:10.1371/journal.pone.0245941 (2021).

7 Evans, W. *et al.* Marine CO_2 Patterns in the Northern Salish Sea. *Frontiers in Marine Science* **5**, doi:https://doi.org/10.3389/fmars.2018.00536 (2019).

8 Campbell, K., Weekes, C., Evans, W., Gimenez, I. & Hales, B. Hakai Institute's Burke-o-Lator TCO_2/pCO_2 Analyzer Discrete Sample Analysis Protocols (v2.0). doi:10.21966/1.521066 (2023).

9 Jiang, L.-Q. *et al.* Best Practices Data Standards for Discrete Chemical Oceanographic Observations. *Frontiers in Marine Science* **8**, 10.3389/fmars.2021.705638 (2022).

10 Newton, J. A., Feely, R. A., Jewett, E. B., Williamson, P. & Mathis, J. Global Ocean Acidification Observing Network: Requirements and Governance Plan *http://goa-on.org/docs/GOA-ON_2nd_edition_final.pdf*, 60 (2015).

11 Wanninkhof, R. & Thoning, K. Measurement of fugacity of CO_2 in surface water using continuous and discrete sampling methods. *Marine Chemistry* **44**, 189-204 (1993).

12 Waters, J., Millero, F. J. & Woosley, R. J. Corrigendum to "The free proton concentration scale for seawater pH", [MARCHE: 149(2013) 8-22]. *Marine Chemistry* **165**, 66-67 (2014).

13 Dickson, A., Wesolowski, D. J., Palmer, D. A. & E., M. R. Dissociation constant of bisulfate ion in aqueous sodium chloride solutions at 250 °C. *Journal of Physical Chemistry* **94**, 7978-7985, doi:doi: 10.1021/j100383a042 (1990).

14 Perez, F. F. & Fraga, F. Association constant of fluoride and hydrogen ions in seawater *Marine Chemistry* **21**, 161-168 (1987).

15 Uppström, L. R. The boron/chlorinity ratio of deep-sea water from the Pacific Ocean. *Deep-Sea Research and Oceanographic Abstracts* **21**, 161-162, doi:doi: 10.1016/0011-7471(74)90074-6 (1974).

16 Sharp, J. D. *et al.* CO2SYSv3 for MATLAB (Version v3.2.0). *Zenodo*, http://doi.org/10.5281/zenodo.3950562 (2021).

17 Orr, J. C., Epitalon, J.-M., Dickson, A. G. & Gattuso, J.-P. Routine uncertainty propagation for the marine carbon dioxide system. *Marine Chemistry* **207**, 84-107, doi:10.1016/j.marchem.2018.10.006 (2018).

18 Hales, B., Suhrbier, A., Waldbusser, G. G., Feely, R. A. & Newton, J. A. The Carbonate Chemistry of the "Fattening Line," Willapa Bay, 2011-2014. *Estuaries and Coasts*, DOI 10.1007/s12237-12016-10136-12237 (2016).

19 Dillon, W. D. N., Dillingham, P. W., Currie, K. I. & McGraw, C. M. Inclusion of uncertainty in the calcium-salinity relationships improves estimates of ocean acidification monitoring data quality. *Marine Chemistry* **226**, 103872 (2020).